A novel pathway for flame synthesis of silica nanoparticles

Shraddha Shekar [1], Markus Sander [1], Rebecca C. Riehl [1], Alastair J. Smith [1],

Andreas Braumann [1], Markus Kraft [1]

released: 21 December, 2010

[1] Department of Chemical Engineering
and Biotechnology
University of Cambridge
New Museums Site
Pembroke Street
Cambridge, CB2 3RA
United Kingdom
E-mail: mk306@cam.ac.uk

Preprint No. 86

UNIVERSITY OF
CAMBRIDGE

Edited by
Computational Modelling Group
Department of Chemical Engineering and Biotechnology
University of Cambridge
New Museums Site
Cambridge CB2 3RA
United Kingdom

Fax:	+ 44 (0)1223 334796
E-Mail:	c4e@cam.ac.uk
World Wide Web:	http://como.ceb.cam.ac.uk/

Abstract

This work proposes a new kinetic model and a novel inception pathway for the flame synthesis of silica nanoparticles from tetraethoxysilane (TEOS). The kinetic model for the decomposition of TEOS is developed by generating reactions involving species that were reported in high concentrations at equilibrium. Flux and sensitivity analyses are then performed to identify the main reaction pathways. The parameters for these reactions are systematically fitted to experimental data using low discrepancy (LD) sequences and response surfaces. The main product of TEOS decomposition is deduced to be silicic acid ($Si(OH)_4$). To increase computational efficiency, the kinetic model has been reduced by determining the level of importance (LOI) of each species and retaining only the important ones. This reduced kinetic model is then coupled to a detailed population balance model using an operator splitting technique. New particle inception and surface growth steps have been incorporated into the particle model in which particles form and grow by the interaction of $Si(OH)_4$ monomers. Coagulation and sintering of particles are also included in the model and the material dependent sintering parameters have been determined by fitting the model to experimental values of collision and primary particle diameters using LD sequences. The particle size distributions and computer generated TEM-style images have been generated and good agreement with experiments is observed. The gas phase reactor composition and the temporal evolution of particle size at different temperatures are also presented.

Contents

1 Introduction

Silica nanoparticles find widespread applications in many fields such as catalysis, chromatography, ceramics, and as stabilising and binding agents [13]. Recent studies have also reported their use in biotechnology for bio-sensing and drug delivery [32]. It has been demonstrated that the rates of gas phase reactions which lead to particle formation are important in determining the final product properties [26], and thus a detailed understanding of these processes is essential.

The formation of silica nanoparticles from tetraethoxysilane (TEOS) using thermal decomposition methods such as flame spray pyrolysis (FSP) is one of the most popular routes for the synthesis of these particles [34]. Despite its industrial importance, the current knowledge of gas-phase decomposition of TEOS to eventually form silica particles remains incomplete. A comprehensive understanding of this process requires the successful coupling of two detailed models: one to determine the kinetics of the gas-phase, and the other to determine the particle dynamics.

Previous kinetic studies conducted in this field suggested that the main reaction pathway for the disintegration of TEOS leads to the formation of silica molecules in the gas-phase. Chu et al. [6] studied the low temperature (700–820 K) decomposition of TEOS and suggested a six-centre decomposition, which formed diethoxy silicate $((C_2H_5O)_2Si=O)$ and equal amounts of ethanol and ethylene. They carried out experiments in the presence of toluene (a chain inhibitor), and these results indicated the possible contributions from a radical-induced mechanism. Takeuchi et al. [35] studied this system in a low pressure chemical vapour deposition reactor at 950 K and 13 Pa and detected the presence of hexaethoxysiloxane $((C_2H_5O)_3Si-O-Si(OC_2H_5)_3)$. They inferred that TEOS reacted with silanol to form hexaethoxysiloxane and ethanol. Herzler et al. [11] studied the decomposition of a few alkoxy silanes (TEOS, tetramethoxysilane (TMOS) and tetrapropoxysilane) using a heated single pulse shock tube and analysed the reactants and final stable products using gas chromatography. The main products were shown to be ethanol and ethylene. They proposed a reaction pathway involving the decomposition of TEOS to form silicates and silyl acids, the rates of which were fitted to their experimental data. This model predicted the activation barrier for the formation of ethanol and silicate from silanol to be less than 200 kJ. However, this is in contrast to the thermochemistry calculated by Ho and Melius [12] using BAC-MP4 methods, where high activation barriers for the formation of ethanol and silicate from silanol were predicted. Their results were consistent with the thermochemistry calculations reported by Phadungsukanan et al. [25] for the TEOS system, where they found the equilibrium concentration of gas-phase silica at atmospheric pressure to be insignificant.

The study of particle dynamics requires an understanding of the following processes: inception, coagulation, surface growth and sintering [21]. Jang [14], Smolík and Moravec [33] and Seto et al. [30] have previously investigated the formation and sintering of silica nanoparticles from TEOS in the vapour phase. Jang [14] synthesised and characterised silica nanoparticles from TEOS vapour in a lab-scale diffusion flame reactor. Seto et al. [30] studied the formation of silica particles in a heated pipe and determined the particle structure and size distribution. Agglomerates were generated at 900 ºC and the change in shape of the particles was evaluated by heating the particles to different final temperatures.

3

Due to the lack of a detailed kinetic model in previous studies, the flame synthesis of silica nanoparticles from TEOS was assumed to proceed via the sticking of gaseous SiO_2 monomers.

The aim of this work is twofold: (i) to develop a new kinetic model which addresses the thermodynamic inconsistencies of the previous models; (ii) to develop a new particle model which incorporates new inception and surface growth steps.

The paper is structured as follows. The kinetic model development for TEOS decomposition is first described in §2. The subsection §2.1 describes the generation of reaction mechanism, §2.2 outlines the optimisation techniques for obtaining the reaction rate parameters and §2.3 discusses the reduction of this kinetic model. The particle model for the formation of silica nanoparticles is described in §3. In subsections §3.1 and §3.2, type space of the particle model and various particle processes are described, followed by the optimisation of free parameters in the particle model in §3.3. The results of the kinetic and particle models are then presented and compared to experimental observations in §3.4. The paper concludes with a discussion of the model's performance and suggests potential improvements to it, along with suitable steps for future research.

2 Kinetic Model

This section outlines the steps involved in the development of a kinetic model for the TEOS system. These steps consist of the generation of a gas phase reaction mechanism, obtaining the optimised rate parameters for these reactions and reducing this comprehensive mechanism to a succinct form suitable to be coupled to population balance equations in §3.

2.1 Gas-phase reaction mechanism

The first step towards generating a reaction mechanism requires the identification of key intermediate species and formulating the possible reactions between them. Each reaction is described by both a forward and a backward rate expression. The rate constant for the forward reaction is usually expressed in modified Arrhenius form:

$$k_{\mathrm{f}} = AT^b \exp(-E_{\mathrm{A}}/RT), \tag{1}$$

where A is the temperature independent pre-exponential factor, b is the temperature coefficient, E_{A} is the activation energy, T is the temperature and R is the universal gas constant. For reversible reactions, the backward rate is calculated from thermochemistry. Thermochemical information is therefore required for each species, and is usually expressed as a polynomial in temperature for specific heat, enthalpy, and entropy [9].

The thermochemistry of over 160 species in the TEOS system is reported Phadungsukanan et al. [25]. Generating a reaction mechanism involving such a large number of species is computationally intractable. It is therefore necessary to make simplifying assumptions as outlined by West et al. [39] in the case of TiO_2 systems. As a first approximation, these thermodynamic equilibrium calculations were used to provide clues

as to which species are most significant, and thus likely to play a prominent role in the reaction mechanism. From the equilibrium graph, the most stable intermediate species in the temperature range 1100–1500 K and at atmospheric pressure were found to be ethoxy and methoxy silanes $(Si(OH)_x(OCH_3)_y(OC_2H_5)_z$, such that $x + y + z = 4)$. The most stable Si species at equilibrium is $Si(OH)_4$, which has an equilibrium mole fraction orders of magnitude higher than any other monomer species. Gaseous SiO_2 is highly unstable at equilibrium, and is thus likely to exist only in very low concentrations. The dimerisation and dehydration of $Si(OH)_4$ is therefore a more favourable route for the formation of silica nanoparticles than the dimerisation of gaseous SiO_2 molecules. The equilibrium calculations were used in this way to identify likely intermediate species and key steps in the reaction mechanism. A preliminary study of bond energies [12] was also performed to indicate the following order of bond strengths: (Si-O) > (O-C) > (C-C).

Based on the results from the equilibrium calculation and the dissociation energies for different bonds in the TEOS molecule, a TEOS decomposition mechanism has been systematically developed. These reaction pathways can be grouped into key categories:

(i) **De-methylation:** Removal of methylene radicals $(:CH_2)$ from adjacent ethoxy groups attached to the central Si atom to form methoxyethoxysilanes $(Si(OH)_x(OCH_3)_y(OC_2H_5)_{4-x-y})$. The TEOS molecule undergoes step-wise de-methylation to subsequently form $Si(OH)_4$ (reactions R1 to R4 in Table 2).

(ii) **De-ethylation:** Removal of terminal C_2H_4 from each ethoxy branch to form ethoxysilanes $(Si(OH)_x(OC_2H_5)_{4-x})$ and ultimately form $Si(OH)_4$ (reactions R15 to R18 in Table 2).

(iii) **De-methylation and disproportionation:** Removal of terminal methyl radicals $(.CH_3)$ to form methoxy silanol radicals $Si(.OCH_2)_x(OC_2H_5)_{4-x}$. These radicals could either undergo a disproportionation reaction to form species with a vinyl group $(-CH=CH_2)$ attached to the central Si atom (reactions R10 to R14 in Table 2). Alternatively, these radicals could undergo further de-methylation to form $Si(OH)_4$ (reactions R5 to R9 in Table 2).

(iv) **De-ethylation and dehydration:** Removal of water or ethanol molecules from ethoxy silanes $Si(OH)_x(OC_2H_5)_{4-x}$ to form the corresponding silicates (-Si=O). The reaction mechanism of Herzler et al. [11] proposes this pathway to form O=Si=O in gas-phase.

The reaction rules listed above have been used to develop a heuristic mechanism to achieve the step wise decomposition of TEOS to eventually form a silicic acid molecule $Si(OH)_4$. The main elementary reaction pathway proposed by Herzler et al. [11] is also included in the mechanism as an alternative route for TEOS decomposition. The full mechanism can be roughly divided into two different sections: the TEOS decomposition with silicon intermediates described above, and C2 carbon chemistry which is based on the ethanol mechanism as proposed by Marinov [17].

All reactions are considered to be reversible to ensure thermodynamic consistency. As a starting point to perform flux and sensitivity analyses in §2.1.1, the rate parameters of the TEOS decomposition reactions are first assumed to have pre-exponential factor, A, as 10^{13}

s^{-1}, and both the temperature coefficient, b, and the activation energy, E_A are assumed to be zero. The rate parameters are then refined by fitting them to experimental data from Herzler et al. [11] in §2.2. The system of ordinary differential equations describing this mechanism is solved using an in-house open source gas-phase chemistry solver written in C++ called *Sprog* [3].

2.1.1 Flux and sensitivity analyses

The analysis of reaction fluxes enables us to draw important conclusions about the underlying chemical mechanism [42]. The instantaneous flux of element Z from species j to species k through reaction i at each reaction time step can be defined as:

$$Z_{i,j,k} = \frac{n_{Z,j} n_{Z,k} r_i}{N_{Z,i}}, \tag{2}$$

where $n_{Z,j}$ and $n_{Z,k}$ are the number of atoms of Z in a molecule of species j and k respectively. $N_{Z,i}$ is the sum of atoms of Z in all species on either side of reaction i and r_i is the rate of reaction i. The instantaneous flux when integrated over the residence time of the reactor gives the time integrated flux. The time integrated flux of element Si for different species involved in TEOS decomposition is calculated for an initial mixture of 420 ppm TEOS in Ar at constant temperature and pressure (1200 °C, 2 bar). The resulting flux diagram is illustrated in **Figure 1**. The thickness of each arrow in this diagram is proportional to the flux associated with the corresponding reaction. Figure 1 shows that the net elemental flux of Si in the direction of Si(OH)$_4$ formation is appreciably higher than in the direction of SiO$_2$ formation.

Sensitivity analysis is a quantitative tool to identify the importance of each reaction in a mechanism resulting in the formation and/or destruction of a given species. In kinetic model development, sensitivities are usually expressed as the logarithmic derivative of species concentration (X_k) with respect to each reaction coefficient A_i. The normalised sensitivity coefficient defined by Miller et al. [20] is calculated as:

$$S_{i,k}(t) = (A_i/X_k^{\max})\frac{\partial X_k(t)}{\partial A_i}, \tag{3}$$

where $S_{i,k}(t)$ is the sensitivity parameter of the kth species with respect to the ith reaction at time t, A_i is the pre-exponential factor of the ith reaction and $X_k(t)$ is the mole fraction of the kth species at a time t.

Sensitivity analysis has been implemented in C++ by solving a system of $N_R(N_S + 1)$ ODEs using the CVODES solver where N_R is the number of reaction species and N_S is the number of parameters with respect to which the sensitivities are to be calculated. Examination of the magnitude and sign of the sensitivity coefficients $S_{i,k}(t)$ provides a useful quantitative tool for assessing the importance of the competing reactions i on the concentration of species k. **Figure 2** depicts the maximum normalised sensitivities of the two main decomposition products, C$_2$H$_4$ and Si(OH)$_4$, for each of the reactions for an initial mixture of 420 ppm TEOS in Ar at constant temperature and pressure (1200 °C, 2 bar). From sensitivity analysis calculations performed in this work, it is apparent that
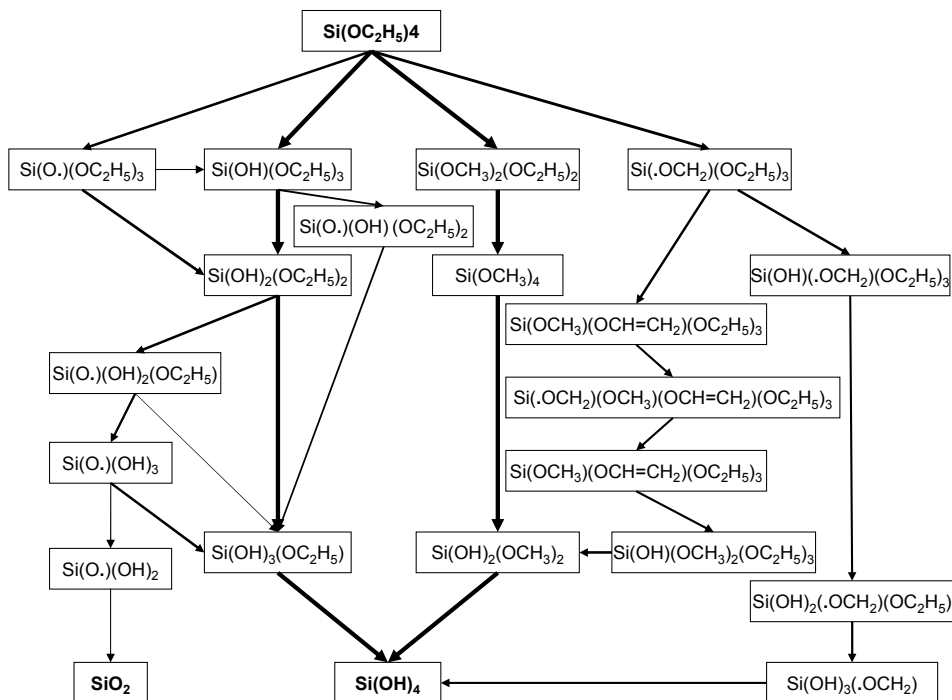
Figure 1: *Integrated flux diagram depicting main reaction pathways.*

the maximum value of the normalised sensitivity parameter for $Si(OH)_4$ and C_2H_4 to re-
actions R1–R10 and R15–R18 (see Table 2) is 10 orders of magnitude higher than that
of elementary reactions proposed by Herzler et al. [11] (R19–R30). Sensitivity to dis-
proportionation reactions of methoxy silanol radicals to form species with vinyl groups
(R11–R14), are also found to be low. Thus, flux and sensitivity analyses have enabled
us to identify the main reaction pathways for which the rate parameters are optimised as
described in §2.2.

2.2 Estimation of rate parameters

To draw meaningful comparisons between model calculations and experimental measure-
ments of species concentration profiles, it is necessary to have an accurate estimate of the
reaction parameter values appearing in the modified Arrhenius expression, Equation 1. A
parameter fitting procedure is therefore adopted in order to reliably estimate these val-
ues, namely, the pre-exponential factor A, and the activation energy E_A. The temperature
coefficient b has been kept at a constant value of zero.

The parameter space of the fitting procedure used in this work has 24 dimensions, and
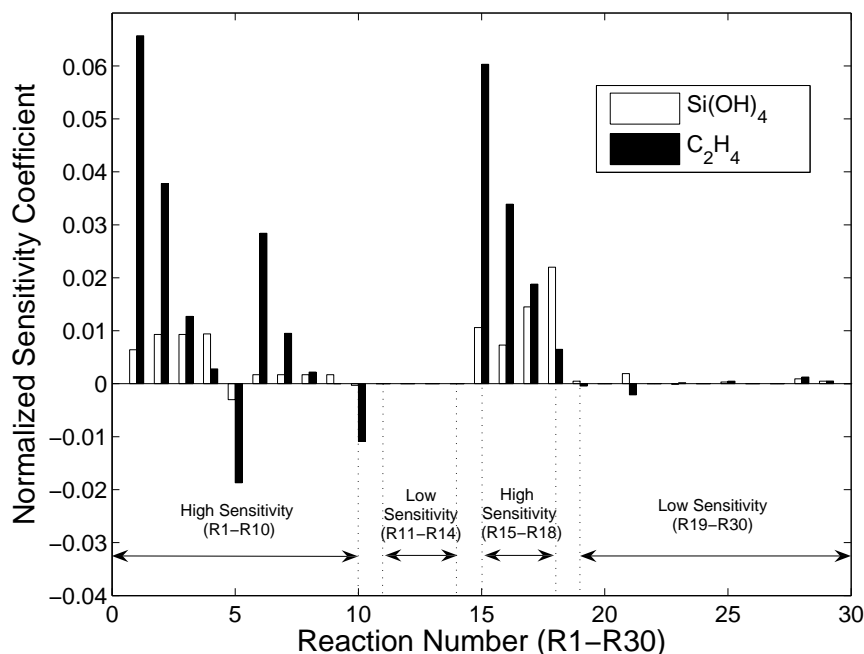
Figure 2: *Maximum normalised sensitivity coefficients for ethylene C_2H_4 and silicic acid $Si(OH)_4$.*

contains elements $\boldsymbol{x}$ of the form

$$\boldsymbol{x} = (A_i, E_{A_j}), \tag{4}$$

where $i \in \{1, \ldots, 18\}$ parameterises the pre-exponential factors, A_i, for each of the 18 reactions and $j \in \{1, \ldots, 6\}$ parameterises the activation energies, E_{A_j}, for each of the 6 bond types.

The parameter fitting consists of the following steps:

(i) Performing a pre-scan of the parameter space using a low discrepancy sequence.

(ii) Construction of a quadratic response surface around the best points from LD sequence using a factorial design to produce a surrogate model.

(iii) Optimisation of the surrogate model to minimise an objective function.

2.2.1 Low discrepancy series

The method of LD series enables us to search for the *best* values of some objective function in a given domain, by doing repetitive evaluations of an objective function at several quasi-random data points in the domain. Data points in the 24-dimensional parameter

space of the current system are generated using a Halton low discrepancy series [10]. The model is then evaluated at these points and the objective function

$$\Phi_1(\boldsymbol{x}) = \sum_{i=1}^{N_{\text{exp}}} \left(\langle Y_i^{\text{exp}} \rangle - \langle Y_i^{\text{sim}} \rangle (\boldsymbol{x}) \right)^2 \tag{5}$$

computed, where N_{exp} is the number of experimental points from Herzler et al. [11]. $\langle Y_i^{\text{exp}} \rangle$ and $\langle Y_i^{\text{sim}} \rangle$ are the experimental and simulated yield of C_2H_4 respectively.

The bounds for the free parameters in the current work were estimated based on physical considerations. For unimolecular reactions these are given by: $10^{11} \leq A_i \leq 10^{18}$, and $0 \leq E_{A_j}/\Delta H_{\text{rxn},j} \leq 10$, where $\Delta H_{\text{rxn},j}$ is the maximum enthalpy of reaction for the jth bond. Due to the large disparity between the upper and lower bounds, logarithmic transformations as described by Braumann et al. [2] have been used, such that

$$x_k = x_{k,\text{up}} \left(\frac{x_{k,\text{low}}}{x_{k,\text{up}}} \right)^{1-h_k}. \tag{6}$$

$h_k \in [0,1]$ is the kth term given by the Halton sequence with $k \in \{1, \dots, K\}$ and K is the number of dimensions. $x_{k,\text{low}}$ and $x_{k,\text{up}}$ are respectively the lower and upper bounds for the kth parameter x_k.

The set of parameters $\boldsymbol{x}$ that minimises this objective function is then determined:

$$\boldsymbol{x}^* = \operatorname*{argmin}_{\boldsymbol{x}} \left\{ \Phi_1(\boldsymbol{x}) \right\}. \tag{7}$$

For this work, a low discrepancy series of 2000 data points in a 24-dimensional space is used to evaluate the objective function $\Phi_1(\boldsymbol{x})$ described by Equation 5 and the set of parameters $\boldsymbol{x}^*$ that minimises $\Phi_1(\boldsymbol{x})$ is determined.

2.2.2 Response Surface Methodology

The next step is the construction of a surrogate model around the best point obtained from the LD series. To facilitate this construction, it is desirable to reduce the dimension of the parameter space, which is realised by performing a sensitivity analysis (as described in §2.1.1). It is found that the model response (concentration of C_2H_4) is most sensitive to the pre-exponential factors (A) and activation energies (E_A) of R1 and R15 defined in Table 2. The normalised sensitivity coefficients of the model response to these reactions are tabulated in **Table 1**.

A surrogate model is then constructed using quadratic response surface methodology in a 4-dimensional space. This methodology has been proposed by Sheen et al. [31] and used by Braumann et al. [1] to optimise a granulation model. Prior to the construction of the surrogate model, it is convenient to perform a logarithmic transformation and normalise the parameter space $\boldsymbol{x}$ to $\tilde{\boldsymbol{x}}$, where $\tilde{x}_k \in \{-1, 0, 1\}$ and $k \in \{1, \dots, 4\}$. The bounds for $\tilde{\boldsymbol{x}}$ are assumed to be $\pm 1\%$. A surrogate model ($\eta(\tilde{\boldsymbol{x}})$) is then constructed and the simulated

9

Table 1: *Normalised sensitivity coefficients of C$_2$H$_4$ concentration with respect to reactions R1 and R15*

Parameter	Normalised sensitivity coefficient
A_1	0.6563
E_{A_1}	1.2237
A_{15}	1.3056
$E_{\mathrm{A}_{15}}$	3.1692

C$_2$H$_4$ yield, $\langle Y_i^{\mathrm{sim}} \rangle(\boldsymbol{x})$ is approximated by a second order response surface as:

$$\langle Y_i^{\mathrm{sim}} \rangle(\boldsymbol{x}) \approx \eta(\tilde{\boldsymbol{x}}) = \beta_0 + \sum_{k=1}^{4} \beta_k \tilde{x}_k + \sum_{k=1}^{4} \sum_{l \geq k}^{4} \beta_{kl} \tilde{x}_k \tilde{x}_l. \tag{8}$$

The coefficients β_0, β_k, and β_{kl} have been fitted by evaluating the model at 81 data points (3 data points for each of the 4 dimensions $= 3^4$ data points). It is assumed that the parameters $\tilde{\boldsymbol{x}}$ are Gaussian distributed and have a mean $\tilde{\boldsymbol{x}}_0$ and a standard deviation $\boldsymbol{c}$:

$$\tilde{\boldsymbol{x}} = \tilde{\boldsymbol{x}}_0 + \boldsymbol{c}\xi, \tag{9}$$

where ξ is Gaussian distributed with mean 0 and variance 1. The Gaussian distribution of the parameters $\tilde{\boldsymbol{x}}$ also influences the model response $\eta(\tilde{\boldsymbol{x}})$. The mean μ can be calculated [1] using:

$$\mu(\tilde{\boldsymbol{x}}_0, \boldsymbol{c}) = \eta(\tilde{\boldsymbol{x}}_0) + \sum_{k=1}^{4} \beta_{kk} c_k^2. \tag{10}$$

It is also possible to express the variance in terms of the coefficients β_0, β_k, and β_{kl} [1]. In contrast to Equation 5, the objective function used in the response surface optimisation also optimises the variances:

$$\Phi_2(\tilde{\boldsymbol{x}}_0, \boldsymbol{c}) = \sum_{i=1}^{N_{\mathrm{exp}}} \left([\langle Y_i^{\mathrm{exp}} \rangle - \mu(\tilde{\boldsymbol{x}}_0, \boldsymbol{c})]^2 + [\sigma_i^{\mathrm{exp}} - \sigma_i(\tilde{\boldsymbol{x}}_0, \boldsymbol{c})]^2 \right). \tag{11}$$

Minimising this objective function leads to the optimal set of parameters:

$$(\tilde{\boldsymbol{x}}_0^*, \boldsymbol{c}^*) = \underset{\tilde{\boldsymbol{x}}_0, \boldsymbol{c}}{\mathrm{argmin}} \left\{ \Phi_2(\tilde{\boldsymbol{x}}_0, \boldsymbol{c}) \right\}. \tag{12}$$

Figure 3 shows the product yield of ethylene as reported experimentally, and that obtained after the response surface optimisation. The bounds of uncertainties for the model response after optimisation are also presented. A relative error of 10% has been assumed for each experimental measurement.

The rate parameters of the TEOS decomposition kinetic model obtained after optimisation are tabulated in **Table 2** alongside their uncertainty bounds. The uncertainties in parameters for Reactions R1 and R15 are calculated using a response surface whilst uncertainties for other reaction parameters are assumed to be the upper and lower bounds of *a priori* values used in RSM.
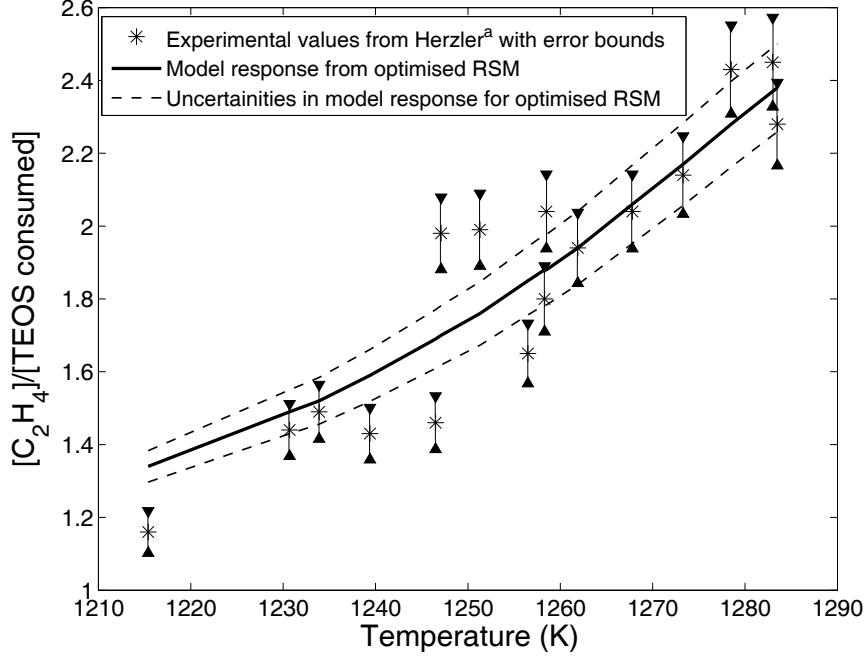
Figure 3: *Optimised model response from response surface methodology and associated uncertainties. [a]Experimental values are from Herzler et al. [11].*

2.3 Gas phase mechanism reduction

Prior to coupling the optimised kinetic model to the stochastic particle model, it is desirable to reduce the chemical mechanism to a concise form to minimise computational times and thus improve efficiency. The mechanism was reduced using the Level of Importance (LOI) technique as introduced by Løvås [16] which combines time scale analysis with a sensitivity analysis with respect to a target parameter. Each species is assigned an LOI parameter, which is defined as:

$$LOI_i^j = S_{i,j} \times \tau_i. \tag{13}$$

where LOI_i^j is the level of importance of species i with respect to parameter j. $S_{i,j}$ is the sensitivity of species i to sensitivity target j and τ_i is the chemical lifetime of species i.

The sensitivity of species i to sensitivity target j is calculated as:

$$S_{i,j} = \left| \frac{\partial X_i}{\partial X_j} \right| \approx \left| \sum_{k=1}^{N_R} \frac{\partial X_i}{\partial A_k} \frac{\partial A_k}{\partial X_j} \right|,$$

where X_i is the mole fraction of species i and X_j is the mole fraction of the target species. For this case, $Si(OH)_4$ was chosen as the target, because this is the product which we seek to accurately model. A_k is the pre-exponential reaction rate parameter of the kth reaction and N_R are total number of reaction.

11

Table 2: *Kinetic model for TEOS decomposition proposed in the current work. The uncertainties in the rate parameters correspond to a relative error of 10% in experimental measurement.*

No.	Reaction Pathway	$\log(A)$ (s^{-1})	b	E_A/R (K^{-1})
R1	$Si(OC_2H_5)_4 \rightleftharpoons Si(OCH_3)_2(OC_2H_5)_2 + C_2H_4$	$12.9 \pm 0.75\%$	0	$26651 \pm 2.87\%$
R2	$Si(OCH_3)_2(OC_2H_5)_2 \rightleftharpoons Si(OCH_3)_4 + C_2H_4$	$12.2 \pm 1\%$	0	$26651 \pm 10\%$
R3	$Si(OCH_3)_4 \rightleftharpoons Si(OH)_2(OCH_3)_2 + C_2H_4$	$12.1 \pm 1\%$	0	$26651 \pm 10\%$
R4	$Si(OH)_2(OCH_3)_2 \rightleftharpoons Si(OH)_4 + C_2H_4$	$11.9 \pm 1\%$	0	$26651 \pm 10\%$
R5	$Si(OC2H5)4 \rightleftharpoons Si(.OCH_2)(OC_2H_5)_3 + .CH_3$	$13.4 \pm 1\%$	0	$49975 \pm 10\%$
R6	$Si(.OCH_2)(OC_2H_5)_3 \rightleftharpoons$ $Si(OH)(.OCH_2)(OC_2H_5)_2 + C_2H_4$	$15.3 \pm 1\%$	0	$27103 \pm 10\%$
R7	$Si(OH)(.OCH_2)(OC_2H_5)_2 \rightleftharpoons$ $Si(OH)_2(.OCH_2)(OC_2H_5) + C_2H_4$	$15.0 \pm 1\%$	0	$27103 \pm 10\%$
R8	$Si(OH)_2(.OCH_2)(OC_2H_5) \rightleftharpoons$ $Si(OH)_3(.OCH_2) + C_2H_4$	$14.8 \pm 1\%$	0	$27103 \pm 10\%$
R9	$Si(OH)_3(.OCH_2) \rightleftharpoons Si(OH)_4 + C_2H_4$	$11.6 \pm 1\%$	0	$44229 \pm 10\%$
R10	$Si(.OCH_2)(OC_2H_5)_3 \rightleftharpoons$ $Si(OCH_3)(OCH=CH_2)(OC_2H_5)_2 + .H$	$14.9 \pm 1\%$	0	$22239 \pm 10\%$
R11	$Si(OCH_3)(OCH=CH_2)(OC_2H_5)_2 \rightleftharpoons$ $Si(.OCH_2)(OCH_3)(OCH=CH_2)(OC_2H_5) + .CH_3$	$12.2 \pm 1\%$	0	$49975 \pm 10\%$
R12	$Si(.OCH_2)(OCH_3)(OCH=CH_2)(OC_2H_5) \rightleftharpoons$ $Si(OCH_3)_2(OCH=CH_2)_2 + .H$	$14.6 \pm 1\%$	0	$22239 \pm 10\%$
R13	$Si(OCH_3)_2(OCH=CH_2)_2 \rightleftharpoons$ $Si(OH)(OCH_3)_2(OCH=CH_2) + C_2H_2$	$15.6 \pm 1\%$	0	$46917 \pm 10\%$
R14	$Si(OH)(OCH_3)_2(OCH=CH_2) \rightleftharpoons$ $Si(OH)_2(OCH_3)_2 + C_2H_2$	$15.3 \pm 1\%$	0	$46917 \pm 10\%$
R15	$Si(OC_2H_5)_4 \rightleftharpoons Si(OH)(OC_2H_5)_3 + C_2H_4$	$14.3 \pm 0.99\%$	0	$31298 \pm 2.88\%$
R16	$Si(OH)(OC_2H_5)_3 \rightleftharpoons Si(OH)_2(OC_2H_5)_2 + C_2H_4$	$14.0 \pm 1\%$	0	$31298 \pm 10\%$
R17	$Si(OH)_2(OC_2H_5)_2 \rightleftharpoons Si(OH)_3(OC_2H_5) + C_2H_4$	$13.9 \pm 1\%$	0	$31298 \pm 10\%$
R18	$Si(OH)_3(OC_2H_5) \rightleftharpoons Si(OH)_4 + C_2H_4$	$13.7 \pm 1\%$	0	$31298 \pm 10\%$

The chemical lifetime of a species τ_i is approximated using the Jacobian matrix [37] as:

$$\tau_i = -\frac{1}{J_{ii}} = \frac{X_i}{\sum_{k=1}^{N}(\nu'_{ik} - \nu''_{ik})\nu'_{ik}\omega_k},$$

where J_{ii} is the diagonal of the Jacobian and $\nu'_{ik} - \nu''_{ik}$ is the net stoichiometric coefficient of species i with respect to parameter k. Rigourous computational singular perturbation (CSP) analysis shows that the eigenvalues of the Jacobian matrix (as described above) give a more exact evaluation of the species' lifetimes [15]. However, the eigenvalues become very similar to the inverse of Jacobian matrix diagonals as the lifetimes get shorter. This allows the two quantities to be used interchangeably with negligible error.

A threshold value for the LOI of each species is defined; if a species has an LOI lower than the threshold, it is excluded from the mechanism. Every reaction associated with that species is also deemed unimportant and thus excluded. The full mechanism prior to reduction, contained 79 species and 401 reactions which can be roughly divided into two different sections: the TEOS decomposition with silicon intermediates, and C2 carbon chemistry. The carbon chemistry was based on the ethanol mechanism as proposed

by Marinov [17]. A skeletal mechanism was developed for process conditions identical to those in experiments by Seto et al. [30] where they synthesised silica nanoparticles in a heated wall reactor at 900 °C with an initial TEOS concentration of 250 ppm and N_2 as the diluent gas. The evolution of important species, such as TEOS, TMOS, C_2H_4, and $Si(OH)_4$, all showed negligible error. This skeletal mechanism containing 27 species and 58 reactions was created using both LOI reduction and elemental flux analysis. The species that were removed using flux analysis were silicon product species whose evolution was orders of magnitude less than $Si(OH)_4$, the main product species. **Figure 4** depicts the concentration profiles of key species with both full and reduced mechanisms and complete agreement is observed between the two.
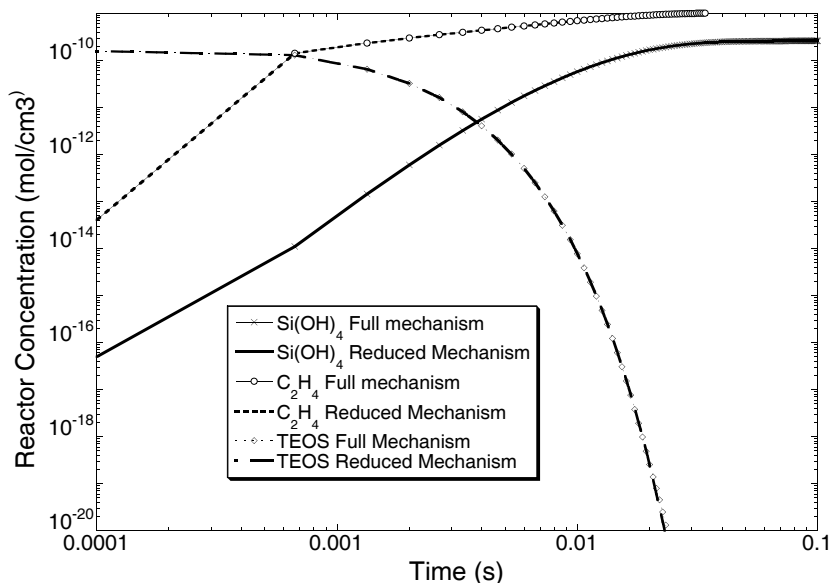

Figure 4: *Species concentration profiles for full mechanism (401 reactions) and reduced mechanism (58 reactions) at experimental conditions of Seto et al. [30].*

The kinetic model for TEOS decomposition obtained after LOI reduction consisting of a silicon submechanism and a hydrocarbon submechanism is provided as supporting material in A.

3   Particle Model

The population balance model which describes the formation of silica nanoparticles is solved using a stochastic particle algorithm developed by Eibeck and Wagner [7] and improved upon by Goodson and Kraft [8] and Patterson and Kraft [22]. This model incorporates submodels that describe particle formation, growth and sintering. The chemical reactions of the precursor (TEOS) leads to the formation of $Si(OH)_4$ monomers (as described in §2) which form particles by inception. These particles grow through surface reactions

13

with monomer, in addition to condensation, coagulation and sintering [21, 27, 28, 38] resulting in the formation of web-like silica nanoparticles. An in-house developed open source solver written in C++ called *MOPS* [3] is used to couple the kinetic model to the particle model. The details of the particle model used in the current work are outlined in this section.

3.1 Type Space

The collection of variables that completely describe the properties of a particle constitute the *type space* of the entity. This is represented by a finite dimensional vector and is defined for the current system by:

$$P_i = P_i(p_1, \ldots, p_n, \mathbf{C}, \mathbf{I}, \mathbf{S}),\tag{14}$$

where $i \in \{1, \ldots, N\}$, and N is the total number of particles in the system. In this model it is assumed that each particle P_i consists of n primary particles p_j, where $j \in \{1, \ldots, n\}$. Both N and n vary with time.

Each primary p_j is described by its volume:

$$p_j = p_j(v_j).\tag{15}$$

The sum of the volumes of all the primaries is equal to the volume V of the particle:

$$V = \sum_{j=1}^{n} v_j.\tag{16}$$

$\mathbf{C}$, $\mathbf{I}$ and $\mathbf{S}$ are square matrices describing the sintering between the primary particles [28]. $[\mathbf{C}]_{i,j}$ contains the common surface of any two primaries p_i and p_j, $[\mathbf{I}]_{i,j}$ contains the sum of the initial surfaces of primary p_i and p_j before sintering and $[\mathbf{S}]_{i,j}$ contains the surface of a sphere with the same volume as primary p_i and p_j. The dimension of these matrices is the number of primaries belonging to the particle.

3.2 Particle processes

The particle can undergo the following processes:

- **Inception:**

  We propose a new particle inception step that proceeds by the interaction of 2 silicic acid molecules resulting in the loss of a water molecule and the formation of a dimer. This dimer is considered to be the first particle. In the current system, collision of two molecules in the gas phase leads to a dehydration reaction. However, in this model, inception has been treated as a coagulation event and a spherical

particle consisting of one primary containing the volume of the two molecules is inserted into the particle ensemble. An inception event increases the total number of particles N by 1:

$$\text{molecule} + \text{molecule} \rightarrow P_{N+1}(p_1, \mathbf{C}, \mathbf{I}, \mathbf{S}). \tag{17}$$
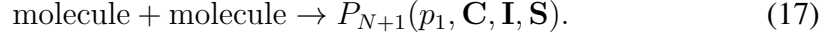
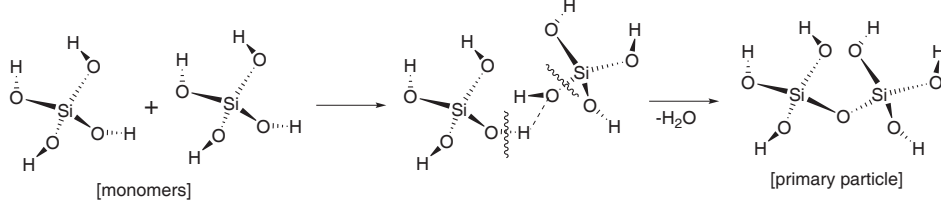This can be represented by a chemical reaction as shown in **Figure 5**.

Figure 5: *Inception of a primary particle from gas-phase monomers.*

For an inception event, the sintering matrices $\mathbf{C}$, $\mathbf{I}$ and $\mathbf{S}$ have dimension 1×1 and the only entry is 0. Due to the small size of the colliding gas-phase monomers, the free molecular kernel has been used to calculate the rate of inception as follows:

$$R_{\text{inception}} = \frac{1}{2} K^{\text{fm}} N_A{}^2 C^2, \tag{18}$$

where K^{fm} is the free molecular regime coagulation kernel constant, N_A is Avogadro's number, C is the gas-phase concentration of the incepting species.

- **Surface Reaction:** A surface reaction is the reaction of a gas-phase molecule (Si(OH)_4) on an active site on a particle P_i as shown in **Figure 6**.
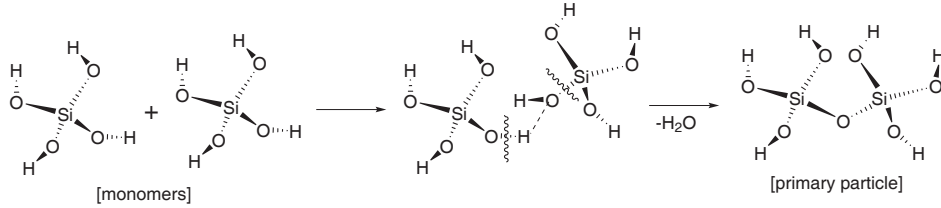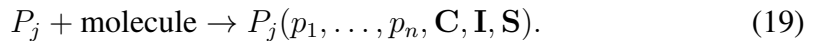

Figure 6: *Surface reaction between a particle and a gas-phase molecule.*

A molecule from the gas-phase collides with a particle, sticks to its surface increasing its mass. In the current model, surface reactions are implemented so that the state space of a particle P_j is altered as follows:

$$P_j + \text{molecule} \rightarrow P_j(p_1, \dots, p_n, \mathbf{C}, \mathbf{I}, \mathbf{S}). \tag{19}$$

This is modelled by increasing the volume of a selected primary p_i of particle P_j as

$$p_i(v) \rightarrow p_i(v + \delta v), \tag{20}$$

15

where δv is the volume of the added gas-phase molecule. The rate of this process is calculated using the free molecular collision kernel for the particle and a single molecule from the gas phase. The rate takes the form

$$R_{\text{surfrxn}} = 2.2\eta C \sqrt{\frac{\pi k_{\text{B}} T}{2m}} \left(d + d_{\text{c}}\right)^2 ,$$ (21)

where C, m and d are the gas-phase concentration, mass and collision diameter of the condensing species respectively. d_{c} is the collision diameter of the particle and η the efficiency of the collision.

- **Coagulation:** The coagulation of particles is the collision and coalescence of two particles P_i and P_j to form a new particle P_k such that the primary particles of the new particle P_k are the same as those of P_i and P_j. This is implemented in the model as:

$$P_i + P_j \rightarrow P_k(p_1, \ldots, p_{n(P_i)}, p_{(n(P_i)+1)}, \ldots, p_{n(P_k)}, \mathbf{C}, \mathbf{I}, \mathbf{S}),$$ (22)

where $n(P_i)$ is the number of primaries belonging to particle P_i and $n(P_k) = n(P_i) + n(P_j)$ the number of primaries belonging to particle P_k. Therefore the number of primary particles l is equal to the number of primaries of particle P_i plus the number of primaries of particle P_j.

The matrices $\mathbf{C}$, $\mathbf{I}$ and $\mathbf{S}$ are updated according to the method described by Sander et al. [28] to represent the connectivity of particles P_i and P_j.

The free molecular collision kernel (equation 23) is used to calculate the coagulation rate between two particles $\mathbf{P}_i$ and $\mathbf{P}_j$.

$$K^{\text{fm}}(i, j) \propto \left(\frac{1}{m(i)} + \frac{1}{m(j)}\right)^{\frac{1}{2}} \left(d_{\text{c}}(i) + d_{\text{c}}(j)\right)^2 ,$$ (23)

where m is the mass and d_{c} the collision diameter. d_{c} of a particle P is calculated as:

$$d_{\text{c}} = \frac{6V}{A} n^{(1/d_{\text{f}})},$$ (24)

where the fractal dimension d_{f} is assumed to be 1.8 [29].

- **Sintering:** The sintering process is modelled by calculating sintering levels for neighbouring primary particles [28]. It is assumed that the excess agglomerate surface area over that of a spherical particle with the same mass decays exponentially [40]. A sintering step reduces the surface area as well as the sphericity of a particle

The sintering level $s(i, j)$ between two primaries p_i and p_j is defined using the equation proposed by Sander et al. [28] as:

$$s(i, j) = \frac{\frac{[\mathbf{S}]_{ij}}{[\mathbf{C}]_{ij}} - \frac{[\mathbf{S}]_{ij}}{[\mathbf{I}]_{ij}}}{1 - \frac{[\mathbf{S}]_{ij}}{[\mathbf{I}]_{ij}}}.$$ (25)

16

The sintering level is updated by calculating the value of matrix **C** for each pair of neighbouring primaries (each non-zero entry of matrix **C**).

$$\frac{d[\mathbf{C}]_{i,j}}{dt} = -\frac{1}{\tau_{\mathrm{s}}} \left([\mathbf{C}]_{i,j} - [\mathbf{S}]_{i,j} \right). \tag{26}$$

The characteristic sintering time τ_{s} is calculated using the formula by Tsantilis et al. [36] as:

$$\tau = A_{\mathrm{S}} \times d_{i,j} \times \exp\left[\frac{E_{\mathrm{S}}}{T} \left(1 - \frac{d_{\mathrm{p,min}}}{d_{i,j}} \right) \right], \tag{27}$$

where $d_{i,j}$ is the minimum diameter of the two neighbouring primaries p_i and p_j. $d_{\mathrm{p,min}}$ is the critical diameter below which the primaries are assumed to be liquid like and they sinter instantaneously. The parameters A_{S}, E_{S} and $d_{\mathrm{p,min}}$ are free parameters in the model. The sintering time is determined by the smallest of two neighbouring primaries [41].

It is assumed that two primaries p_i and p_j are completely sintered if the sintering level $s(i,j)$ (Equation 25) is greater than 0.95. This is included in the model by replacing primary p_i and p_j by a new primary p_k. The volume of the new primary p_k is the sum of the volumes of the primaries p_i and p_j and the neighbouring primaries of the new primary p_k are the neighbours of the primaries p_i and p_j.

The particles processes described above are implemented for an ensemble of stochastic particles using a Linear Process Deferment Algorithm [23]. The kinetic model described in §2 and the particle model described in this section are coupled using an operator splitting technique developed by Celnik et al. [4, 5] to generate the overall model.

3.3   Estimation of sintering parameters

The material dependant sintering parameters A_{S}, E_{S} and $d_{\mathrm{p,min}}$ in Equation 27 have been determined by fitting the model to the experiments of Seto et al. [30] who generate silica particles at 900 °C and observe the change in primary and collision diameters by heating the particles to 6 different final temperatures. The simulation used to reproduce this experiment involves: (i) decomposition of TEOS to generate monomers and formation of particles in the first reactor at 900 °C from an initial gas mixture of TEOS and N_2; (ii) heating the particles within 0.1 s to different final temperatures T_{f}; (iii) allowing the particles to remain at temperature T_{f} for a certain period of time.

The sintering parameters are optimised using a low discrepancy series as described in §2.2. The 3-dimensional parameter space is given by:

$$\boldsymbol{y} = (A_{\mathrm{S}}, E_{\mathrm{S}}, d_{\mathrm{p,min}}). \tag{28}$$

The objective function is given by:

$$\Phi(\boldsymbol{y}) = \sum_{i=1}^{N_{\mathrm{exp}}} \left([\langle d_{\mathrm{c}_i}^{\mathrm{exp}} \rangle - \langle d_{\mathrm{c}_i}^{\mathrm{sim}} \rangle(\boldsymbol{y})]^2 + [\langle d_{\mathrm{p}_i}^{\mathrm{exp}} \rangle - \langle d_{\mathrm{p}_i}^{\mathrm{sim}} \rangle(\boldsymbol{y})]^2 \right), \tag{29}$$

where N_{exp} is the number of experimental points from Seto et al. [30]. $\langle d_{\text{c}_i}^{\text{exp}} \rangle$, $\langle d_{\text{p}_i}^{\text{exp}} \rangle$, $\langle d_{\text{c}_i}^{\text{sim}} \rangle$ and $\langle d_{\text{p}_i}^{\text{sim}} \rangle$ are the experimental and simulated collision and primary particle diameters respectively. The set of parameters that minimises Equation 29 is determined as:

$$\boldsymbol{y}^* = \underset{\boldsymbol{y}}{\text{argmin}} \left\{ \Phi(\boldsymbol{y}) \right\}. \tag{30}$$

In this work, 2000 data points are generated using Halton low discrepancy series [10] in the 3-dimensional parameter space given by $\boldsymbol{y}$. The objective function $\Phi(\boldsymbol{y})$ is evaluated at these data points and the set of parameters $\boldsymbol{y}^*$ that minimises $\Phi(\boldsymbol{y})$ is determined. The resulting values of $\boldsymbol{y}^*$ are shown in **Table 3** and are similar to those reported by Sander et al. [28]. The under-prediction in the value of A_{S} is envisaged to be due to the inclusion of the actual chemistry of TEOS decomposition in the particle model, which leads to an increase in the residence time of the reactor.

Table 3: *Values of sintering parameters in the particle model compared to values calculated by Sander et al. [28].*

Parameter	Value (current model)	Value [28]
A_{S} (m^{-1}s)	1.16×10^{-16}	6.5×10^{-15}
E_{S} (K)	12.7×10^4	10.2×10^4
$d_{\text{p,min}}$ (m)	4.4×10^{-9}	10.2×10^{-9}

The optimised model response, i.e. the average collision diameter and particle diameter at different final temperatures is shown in **Figure 7**. The model response using full and reduced mechanisms (§2.3) are also compared and perfect agreement is observed between the two.

3.4 Analysis of results

The values of the free parameters in §3.3 have been estimated by fitting the model to the experimental values of only average primary and collision diameters from Seto et al. [30]. To establish the consistency of the model with experiments, in this subsection we analyse various other model results and compare them with experimental observations.

Gas phase reactor composition

The time evolution of the prominent gaseous silicon species in the reactor for the first 100 ms is shown in **Figure 8**. The first reactor is at constant temperature and pressure (900 °C, 1.01 bar) with an initial mixture of 250 ppm TEOS in N_2. The residence time t_{r} in the first reactor is set to 1 s in the following simulations.

Figure 8 suggests that reaction proceeds via the step-wise decomposition of TEOS to form ethoxy or methoxy silanols as intermediates which undergo further decomposition to ultimately form $Si(OH)_4$. These $Si(OH)_4$ monomers act as seeds for particle formation and are rapidly consumed from the gas phase to particulate phase.
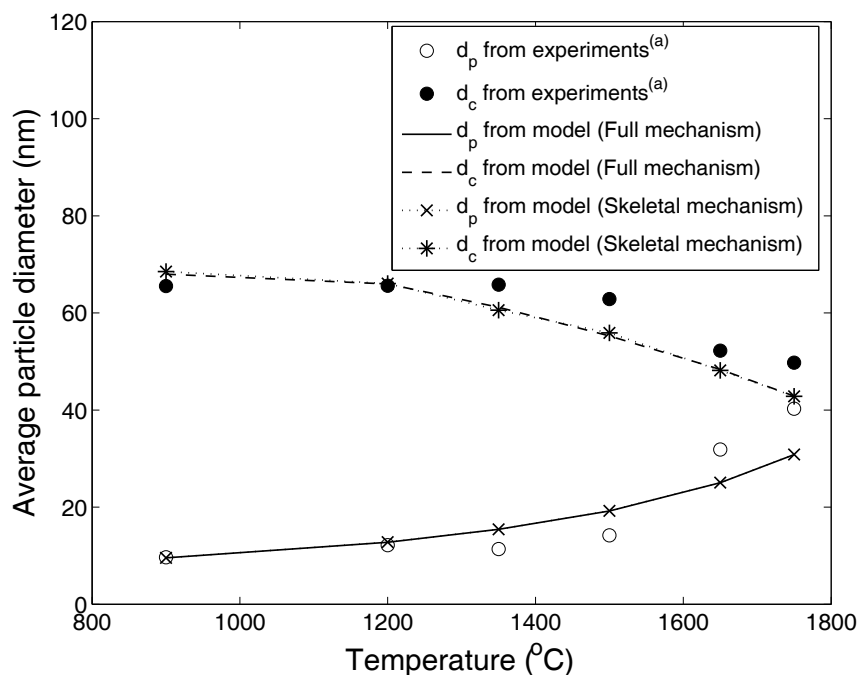
Figure 7: *Optimised model response, i.e. average primary diameter (d_p) and collision diameter (d_c) at different final temperatures. [a]Experimental values are from Seto et al. [30].*

Temporal evolution of particle size

Chemical reactions in gas-phase occur in the first reactor and $Si(OH)_4$ monomers are formed as depicted in Figure 8. In the first reactor, particle formation occurs as a result of collision of two silicic acid molecules to form one primary particle with the volume of the formed dimer. When introduced into the second reactor at high temperature, the particles rapidly start to sinter. The time evolution of particles at different final temperatures (T_f) is shown in **Figure 9**. In the first reactor at a temperature of 900 °C, the primary particles, once formed, remain constant in size. However, as the particles are introduced in the second reactor, the primary particle diameter rapidly increases indicating greater levels of sintering at higher temperatures. The collision diameter of the particle increases in the first reactor due to surface reaction and coagulation. As soon as the particles are introduced in the second reactor, the sintering process predominates, reducing the overall size of the particle. At a temperature of about 2000 °C, the collision diameter and primary diameter become identical and particles become spherical, thus no further sintering is possible.

Particle size distributions

The size distributions with respect to primary particle diameter (d_p) and collision diameter (d_c) at three different final temperatures are given in **Figure 10**. At 900 °C, the primary particle size distribution has a small standard deviation and mean. As the furnace tempera-
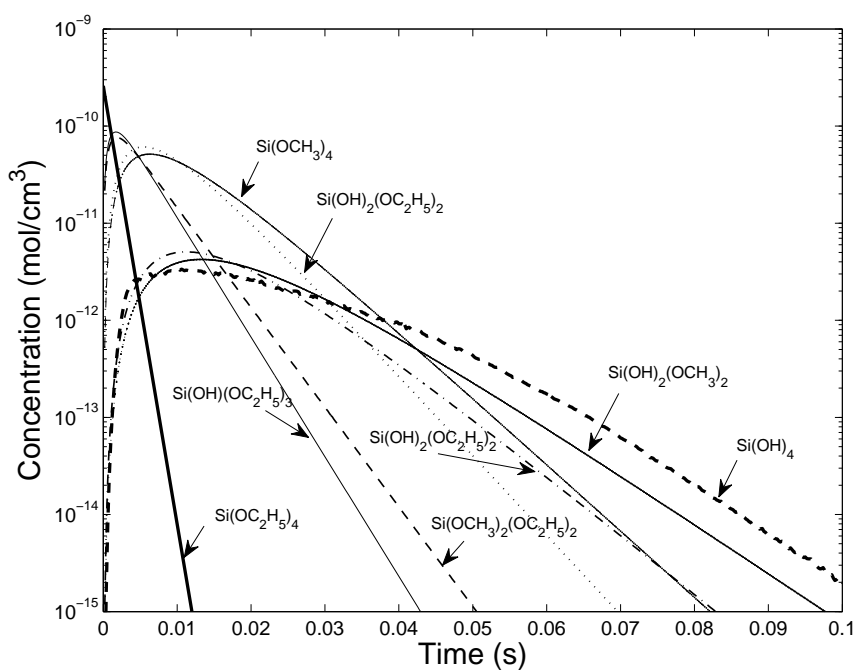
Figure 8: *Gas phase reactor composition versus time. Initial composition is 250 ppm TEOS in N_2, T=900 °C and P=1.01 bar.*
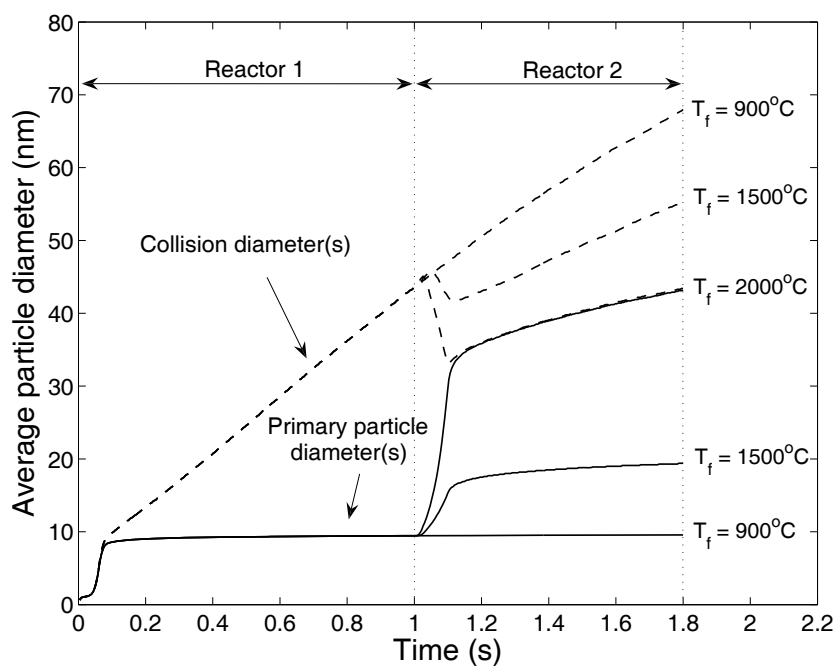

Figure 9: *Time evolution of average particle size at different final temperatures.*

20

ture increases, the mean and standard deviation also increase. The corresponding collision diameter distribution gets narrower with increasing temperature due to the sintering of the particles. In the comparison it is assumed that the mobility diameter (experimental values from Seto et al. [30]) is equal to the collision diameter.
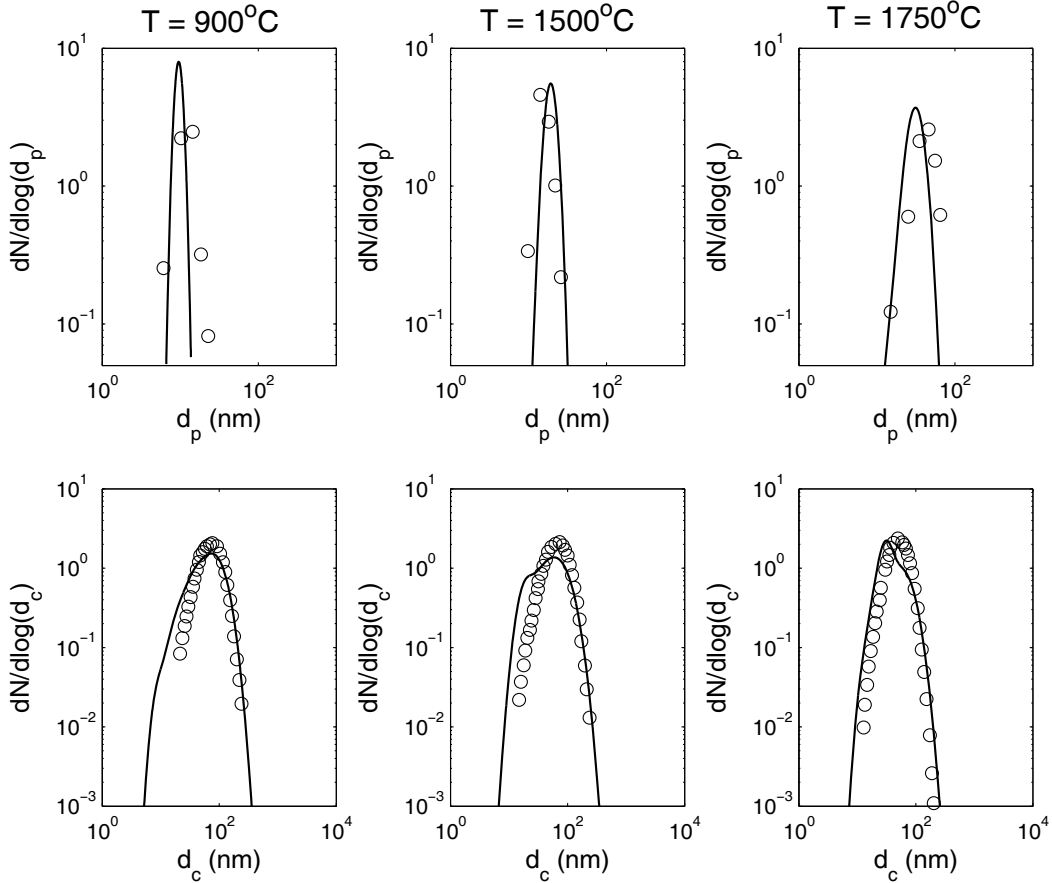

Figure 10: *Particle size distribution at different furnace temperatures. The circles are experimental points from Seto et al. [30] and the solid lines are from simulation.*

Computer generated TEM images

The computer TEM images are generated by assuming that each particle is created by sticking together its constituting primary particles in a random fashion. These particles are projected onto a plane to simulate a collection of particles as generated using a TEM grid in an experiment. Computer generated TEM style images are compared to experimental values from Seto et al. [30] as demonstrated in **Figure 11**. From Figure 11, it is apparent that the particles reduce in size with increasing temperature and become rounder. The particles are nearly spherical at 1750 °C. The particle size distributions and the TEM images calculated by the model are found to be in close agreement with the experimental data.
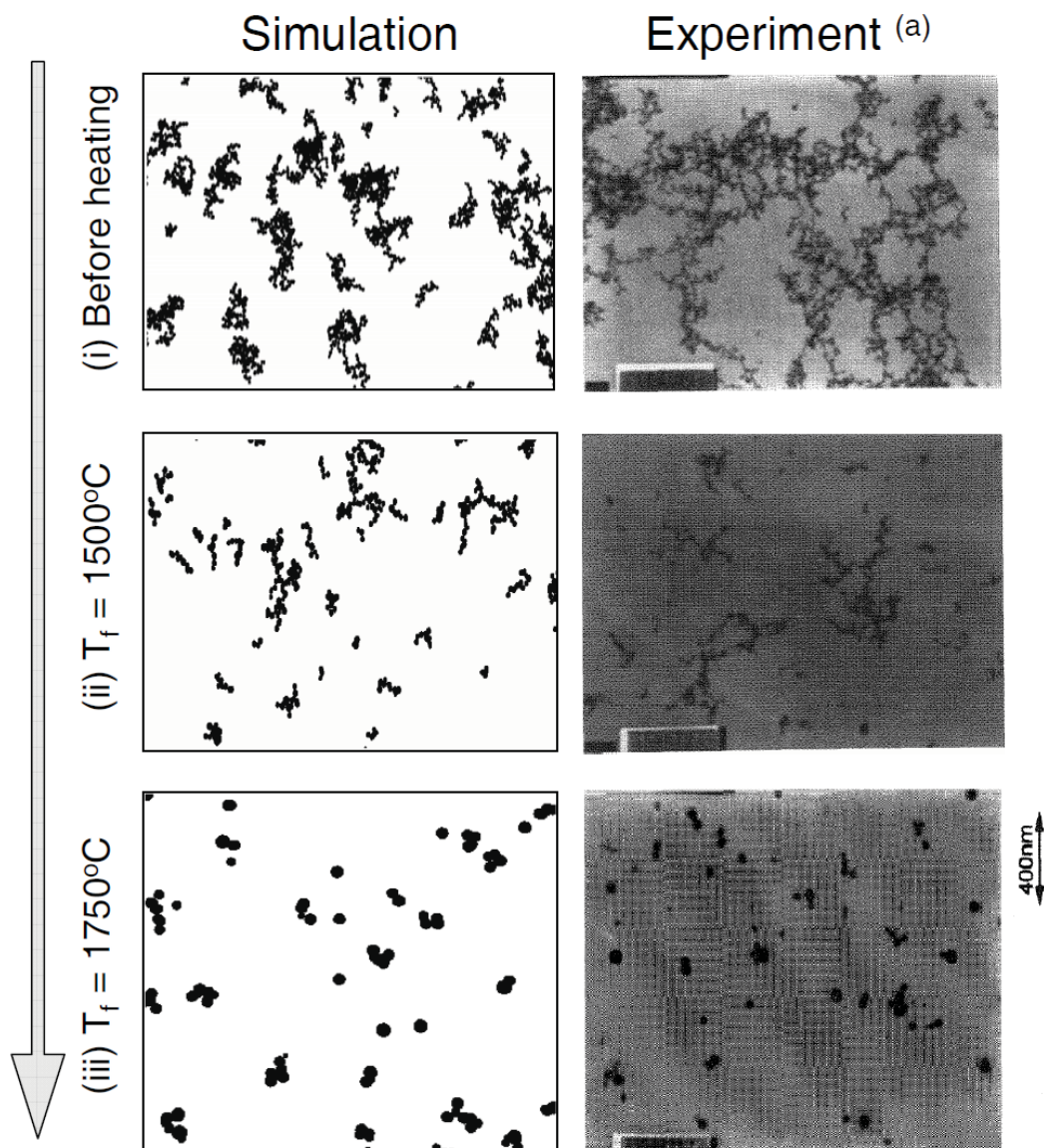
Figure 11: *TEM style images at different final temperatures from simulation and experiment. (a)Experimental images are from Seto et al. [30].*

4 Conclusion

A comprehensive model has been generated for the flame synthesis of silica nanoparticles from TEOS. Using recently published thermochemical data for the TEOS intermediates, the present work outlines a thermodynamically consistent kinetic model for decomposition of TEOS generated from first principles. Initially, a rudimentary kinetic model was constructed which was found to be at least qualitatively correct, and suggested that silicic acid $Si(OH)_4$ was the main product of the decomposition. Flux and sensitivity analyses were used to identify the dominant reaction pathways, which led to the conclusion that

the decomposition of TEOS to form silicates is insignificant under the process conditions of current work. The model predictions, i.e., the final product concentrations, were sensitive to the assumed pre-exponential rate parameters, and therefore, in order to improve the performance of the model, rate parameter optimisation was carried out. Low discrepancy series and response surface methodology were applied in order to estimate the rate parameters of the model and to determine the uncertainties in model parameters given the experimental error. A detailed transition state search analysis is an essential next step in order to determine exact values of the rate parameters.

The kinetic model developed was then coupled to a stochastic particle model that includes the processes through which $Si(OH)_4$ monomers ultimately form silica aggregates. The material dependent sintering parameters in the particle model were estimated by fitting the model to experimental values of collision and primary particle diameters using low discrepancy series. The particle size distributions and computer-generated TEM images at different temperatures were compared with experimental values and good agreement was found. Work is currently underway to develop a detailed population balance model, where the particle jump processes are considered in conjunction with chemical reactions and the chemical units (i.e., numbers of Si, O and H units) within each particle in the population are tracked.

By coupling a new kinetic model, generated from quantum chemical calculations, to a new population balance model with primary particle tracking, the current work demonstrates the feasibility of using first-principles modelling to understand complex particle synthesis processes.

5 Acknowledgments

References

[1] A. Braumann, P. L. W. Man, and M. Kraft. Statistical approximation of the inverse problem in multivariate population balance modelling. *Ind. Eng. Chem. Res.*, 49(1): 428–438, 2010. doi:10.1021/ie901230u.

[2] A. Braumann, P. L. W. Man, and M. Kraft. The inverse problem in granulation modelling - two different statistical approaches. *AIChE J*, In press, 2011.

[3] M. S. Celnik. *On the numerical modelling of Soot and Carbon Nanotube Formation*. PhD thesis, University of Cambridge, 2007.

[4] M. S. Celnik, R. I. A. Patterson, M. Kraft, and W. Wagner. Coupling a stochastic soot population balance to gas-phase chemistry using operator splitting. *Combust. Flame*, 148(3):158–176, 2007. doi:10.1016/j.combustflame.2006.10.007.

[5] M. S. Celnik, R. I. A. Patterson, , M. Kraft, and W. Wagner. A predictor-corrector algorithm for the coupling of stiff odes to a particle population balance. *J. Comp. Phys.*, 228(8):2758–2769, 2009. doi:10.1016/j.jcp.2008.12.030.

[6] J. C. Chu, J. Breslin, N. Wang, and M. Lin. Relative stabilities of tetramethyl orthosilicate and tetraethyl orthosilicate in the gas phase. *Mater. Lett.*, 12(3):179–184, 1991. doi:10.1016/0167-577X(91)90170-B.

[7] A. Eibeck and W. Wagner. An efficient stochastic algorithm for studying coagulation dynamics and gelation phenomena. *SIAM J. Sci. Comput.*, 22(3):802–821, 2000. doi:10.1137/S1064827599353488.

[8] M. Goodson and M. Kraft. An efficient stochastic algorithm for simulating nano-particle dynamics. *J. Comput. Phys.*, 183(1):210–232, 2002. doi:10.1006/jcph.2002.7192.

[9] S. Gordon and B. J. McBride. Computer program for calculation of complex chemical equilibrium composition, rocket performance, incident and reflected shocks and chapman-jouget detonations. Technical report, NASA Washington DC, 1976.

[10] J. H. Halton. On the efficiency of certain quasi-random sequences of points in evaluating multi-dimensional integrals. *Numer. Math.*, 2(1):84–90, 1960. doi:10.1007/BF01386213.

[11] J. Herzler, J. A. Manion, and W. Tsang. Single-Pulse Shock Tube Study of the Decomposition of Tetraethoxysilane and Related Compounds. *J. Phys. Chem. A*, 101(30):5500–5508, 1997. doi:10.1021/jp9706543.

[12] P. Ho and C. F. Melius. Theoretical Study of the Thermochemistry of Molecules in the Si-O-H-C System. *J. Phys. Chem.*, 99(41):2166–2176, 1995. doi:10.1021/j100007a056.

[13] R. K. Iler. *The Chemistry of Silica: Solubility, Polymerization, Colloid and Surface Properties and Biochemistry of Silica*. WILEY, Toronto, Canada, 1979. ISBN 978-0-471-02404-0.

[14] H. D. Jang. Generation of silica nanoparticles from tetraethylorthosilicate (TEOS) vapor in a diffusion flame. *Aerosol Sci. Tech.*, 30(5):477–488, 1999. doi:10.1080/027868299304516.

[15] S. H. Lam and D. A. Goussis. The CSP method for simplifying kinetics. *Int. J. Chem. Kin.*, 26(4):461–486, 1994. doi:10.1002/kin.550260408.

[16] T. Løvås. Automatic generation of skeletal mechanisms for ignition combustion based on level of importance analysis. *Combust. Flame*, 156(7):1348–1358, 2009. doi:10.1016/j.combustflame.2009.03.009.

[17] N. M. Marinov. A detailed chemical kinetic model for high temperature ethanol oxidation. *Int. J. Chem. Kin.*, 31(3):183–220, 1999. doi:10.1002/(SICI)1097-4601(1999)31:3<183::AID-KIN3>3.0.CO;2-X.

[18] N. M. Marinov, W. J. Pitz, C. K. Westbrook, M. J. Castaldi, and S. M. Senkan. Modeling of aromatic and polycyclic aromatic hydrocarbon formation in premixed methane and ethane flames. *Comb. Sci. Tech.*, 116(1):211–287, 1996. doi:10.1080/00102209608935550.

[19] N. M. Marinov, M. J. Castaldi, C. F. Melius, and W. Tsang. Aromatic and polycyclic aromatic hydrocarbon formation in a premixed propane flame. *Comb. Sci. Tech.*, 128 (1):295–342, 1997. doi:10.1080/00102209708935714.

[20] J. A. Miller, M. C. Branch, W. J. McLean, D. W. Chandler, M. D. Smooke, and R. J. Kee. The conversion of HCN to NO and N_2 in H_2-O_2-HCN-AR flames at low pressure. *Intl. Symp. Comb.*, 20(1):673–684, 1985. doi:10.1016/S0082-0784(85)80557-9.

[21] N. Morgan, C. Wells, M. Kraft, and W. Wagner. Modelling nanoparticle dynamics: Coagulation, sintering, particle inception and surface growth. *Combust. Theor. Model.*, 9(3):449–461, 2005. doi:10.1080/13647830500277183.

[22] R. I. A. Patterson and M. Kraft. Models for the aggregate structure of soot particles. *Combust. Flame*, 151(1):160–172, 2007. doi:10.1016/j.combustflame.2007.04.012.

[23] R. I. A. Patterson, J. Singh, M. Balthasar, M. Kraft, and J. Norris. The Linear Process Deferment Algorithm: A new technique for solving population balance equations. *SIAM J. Sci. Comput.*, 28(1):303–320, 2006. doi:10.1137/040618953.

[24] J. F. Pauwels, J. V. Volponi, and J. A. Miller. The oxidation of allene in a low-pressure H_2/O_2/AR-C_3H_4 flame. *Comb. Sci. Tech.*, 110(11):249–276, 1995. doi:10.1080/00102209508951926.

[25] W. Phadungsukanan, S. Shekar, R. Shirley, M. Sander, R. H. West, and M. Kraft. First-principles thermochemistry for silicon species in the decomposition of tetraethoxysilane. *J. Phys. Chem. A*, 113(31):9041–9049, 2009. doi:10.1021/jp905494s.

[26] S. E. Pratsinis. Simultaneous nucleation, condensation, and coagulation in aerosol reactors. *J. Colloid Interface Sci.*, 124(2):416–428, 1988. doi:10.1016/0021-9797(88)90180-4.

[27] S. E. Pratsinis and S. Vemury. Particle formation in gases: a review. *Powder Technol.*, 88(3):267–273, 1996. doi:10.1016/S0032-5910(96)03130-0.

[28] M. Sander, R. H. West, M. S. Celnik, and M. Kraft. A detailed model for the sintering of polydispersed nanoparticle agglomerates. *Aerosol Sci. Tech.*, 43(10):978–989, 2009. doi:10.1080/02786820903092416.

[29] D. W. Schaefer and A. J. Hurd. Growth and structure of combustion aerosols: fumed silica. *Aerosol Sci. Tech.*, 12(4):876–890, 1990. doi:10.1080/02786829008959400.

[30] T. Seto, A. Hirota, T. Fujimoto, M. Shimada, and K. Okuyama. Sintering of Polydisperse Nanometer-Sized Agglomerates. *Aerosol Sci. Tech.*, 27(3):422–438, 1997. doi:10.1080/02786829708965482.

[31] D. A. Sheen, X. You, H. Wang, and T. Løvås. Spectral uncertainty quantification, propagation and optimization of a detailed kinetic model for ethylene combustion. *Proc. Combust. Inst.*, 32(1):535–542, 2009. doi:10.1016/j.proci.2008.05.042.

[32] I. I. Slowing, B. G. Trewyn, S. Giri, and V. S.-Y. Lin. Mesoporous silica nanoparticles for drug delivery and biosensing applications. *Adv. Funct. Mater.*, 17(8):1225–1236, 2007. doi:10.1002/adfm.200601191.

[33] J. Smolík and P. Moravec. Gas phase synthesis of fine silica particles by oxidation of tetraethylorthosilicate vapour. *J. Mater. Sci. Lett.*, 14(6):387–488, 1995. doi:10.1007/BF00274548.

[34] W. J. Stark and S. E. Pratsinis. Aerosol flame reactors for manufacture of nanoparticles. *Chem. Eng. Prog.*, 126(2):103–108, 2002. doi:10.1016/S0032-5910(02)00077-3.

[35] H. Takeuchi, H. Izami, and A. Kawasaki. Decomposition study on TEOS. *Mater. Res. Soc. Symp. Proc.*, 334(1):45–55, 1994.

[36] S. Tsantilis, H. Briesen, and S. E. Pratsinis. Sintering time for silica particle growth. *Aerosol Sci. Tech.*, 34(3):237–246, 2001.

[37] T. Turányi, A. S. Tomlin, and M. J. Pilling. On the error of the quasi-steady-state approximation. *J. Phys. Chem.*, 97(1):163–172, 1993.

[38] G. D. Ulrich. Theory of particle formation and growth in oxide synthesis flames. *Comb. Sci. Tech.*, 4(1):47–57, 1971. doi:10.1080/00102207108952471.

[39] R. H. West, M. S. Celnik, O. R. Inderwildi, M. Kraft, G. J. O. Beran, and W. H. Green. Towards a comprehensive model of the synthesis of TiO_2 particles from $TiCl_4$. *Ind. Eng. Chem. Res.*, 46(19):6147–6156, 2007. doi:10.1021/ie0706414.

[40] Y. Xiong and S. E. Pratsinis. Formation of agglomerate particles by coagulation and sinterings – part I. A two-dimensional solution of the population balance equation. *J. Aerosol Sci.*, 24(3):283–300, 1993. doi:10.1016/0021-8502(93)90003-R.

[41] V. Yadha and J. Helble. Modeling the coalescence of heterogenous amorphous particles. *J. Aerosol Sci.*, 35(6):665–681, 2004. doi:10.1016/j.jaerosci.2003.11.009.

[42] I. G. Zsély, I. Virág, and T. Turányi. Investigation of a methane oxidation mechanism via the visualization of element fluxes. Technical report, Department of Physical Chemistry, Eötvös University (ELTE), Budapest, Hungary, 2005. URL http://garfield.chem.elte.hu/turanyi/pdf/77_Zsely_Lisbon_2005.pdf.

A Appendix

A.1 Reaction Mechanism for TEOS decomposition

Table 4 depicts the skeletal mechanism for the gas phase decomposition of TEOS with N_2 as a diluent. The reduced mechanism consists of 58 reactions and 27 species.

Table 4: *Reaction mechanism for TEOS decomposition. The references marked [*] are reactions proposed in this study.*

No.	Reaction Pathway	$\log(A)$	b	$E_A/R\ (K^{-1})$	Reference
	Si Submechanism				
1	$Si(OC_2H_5)_4 \rightleftharpoons Si(OCH_3)_2(OC_2H_5)_2 + C_2H_4$	12.5	0	26651	[*]
2	$Si(OCH_3)_2(OC_2H_5)_2 \rightleftharpoons Si(OCH_3)_4 + C_2H_4$	12.2	0	26651	[*]
3	$Si(OCH_3)_4 \rightleftharpoons Si(OH)_2(OCH_3)_2 + C_2H_4$	12.1	0	26651	[*]
4	$Si(OH)_2(OCH_3)_2 \rightleftharpoons Si(OH)_4 + C_2H_4$	11.9	0	26651	[*]
5	$Si(OC2H5)4 \rightleftharpoons Si(OH)(OC_2H_5)_3 + C_2H_4$	14.3	0	31298	[*]
6	$Si(OH)(OC_2H_5)_3 \rightleftharpoons Si(OH)_2(OC_2H_5)_2 + C_2H_4$	14.0	0	31298	[*]
7	$Si(OH)_2(OC_2H_5)_2 \rightleftharpoons Si(OH)_3(OC_2H_5) + C_2H_4$	13.9	0	31298	[*]
8	$Si(OH)_3(OC_2H_5) \rightleftharpoons Si(OH)_4 + C_2H_4$	13.7	0	31298	[*]
	Hydrocarbon Submechanism				
9	$H + H + M \rightleftharpoons H_2 + M$	12	-1	0	[18]
10	$H + H + H_2 \rightleftharpoons H_2 + H_2$	11	-1	0	[18]
11	$CH_3 + H + M \rightleftharpoons CH_4 + M$	15	0	0	[18]
	Low pressure limit	31	-4	1061	
	Troe Parameters: a = 0, T*** = 1.00E-15,				
	T* = 1.00E-15, T** = 40				
12	$CH_4 + H \rightleftharpoons CH_3 + H_2$	4	3	4406	[18]
13	$CH_3 + H \rightleftharpoons CH_2 + H_2$	14	0	7604	[18]
14	$CH_3 + M \rightleftharpoons CH + H_2 + M$	15	0	41528	[18]
15	$CH_3 + M \rightleftharpoons CH_2 + H + M$	16	0	46031	[18]
16	$CH_2 + H \rightleftharpoons CH + H_2$	18	-2	0	[18]
17	$CH_2 + CH_3 \rightleftharpoons C_2H_4 + H$	14	0	0	[18]
18	$CH_2 + CH_2 \rightleftharpoons C_2H_2 + H$	14	0	0	[18]
19	$CH_2 + C_2H_2 \rightleftharpoons H_2CCCH + H$	13	0	3323	[18]
20	$CH_2(S) + M \rightleftharpoons CH_2 + M$	13	0	0	[18]
21	$CH_2(S) + CH_4 \rightleftharpoons CH_3 + CH_3$	14	0	0	[18]
22	$CH_2(S) + H_2 \rightleftharpoons CH_3 + H$	14	0	0	[18]
23	$CH_2(S) + C_2H_2 \rightleftharpoons H_2CCCH + H$	14	0	0	[18]
24	$CH_2(S) + C_2H_4 \rightleftharpoons AC_3H_5 + H$	14	0	0	[18]
25	$CH_2(S) + H \rightleftharpoons CH + H_2$	13	0	0	[18]
26	$CH_2(S) + CH_3 \rightleftharpoons C_2H_4 + H$	13	0	0	[18]
27	$CH + C_2H_2 \rightleftharpoons C_3H_2 + H$	14	0	0	[18]
28	$CH + CH_2 \rightleftharpoons C_2H_2 + H$	14	0	0	[18]

(continued)

No.	Reaction Pathway	$\log(A)$	b	E_A/R (K^{-1})	Reference
29	$CH + CH_3 \rightleftharpoons C_2H_3 + H$	13	0	0	[18]
30	$CH + CH_4 \rightleftharpoons C_2H_4 + H$	14	0	0	[18]
31	$C_2H_5 + H \rightleftharpoons C_2H_4 + H_2$	14	0	4028	[18]
32	$C_2H_5 + H \rightleftharpoons CH_3 + CH_3$	13	0	0	[18]
33	$C_2H_4 + CH_3 \rightleftharpoons C_2H_3 + CH_4$	1	4	4784	[18]
34	$C_2H_4 + H \rightleftharpoons C_2H_3 + H_2$	-6	6	852	[18]
35	$C_2H_4 + H + M \rightleftharpoons C_2H_5 + M$	12	0	917	[18]
	Low pressure limit	34	-5	2240	
	Troe Parameters: a = 1, T*** = 1.00E-15,				
	T* = 95, T** = 200				
36	$C_2H_4 \rightleftharpoons C_2H_2 + H_2$	5	0	0	[18]
37	$C_2H_3 + H + M \rightleftharpoons C_2H_4 + M$	13	0	141	[18]
	Low pressure limit	30	-4	1672	
	Troe Parameters: a = 0.782, T*** = 208,				
	T* = 2663, T** = 6095				
38	$C_2H_3 + H \rightleftharpoons C_2H_2 + H_2$	14	0	0	[18]
39	$C_2H_3 + C_2H \rightleftharpoons C_2H_2 + C_2H_2$	13	0	0	[18]
40	$C_2H_3 + CH \rightleftharpoons CH_2 + C_2H_2$	14	0	0	[18]
41	$C_2H_3 + CH_3 \rightleftharpoons AC_3H_5 + H$	3	4	2859	[18]
42	$C_2H_3 + CH_3 \rightleftharpoons C_3H_6$	57	-13	6982	[18]
43	$C_2H_3 + CH_3 \rightleftharpoons C_2H_2 + CH_4$	13	0	0	[18]
44	$C_2H_2 + CH_3 \rightleftharpoons C_2H + CH_4$	11	0	8706	[18]
45	$C_2H_2 + M \rightleftharpoons C_2H + H + M$	17	0	53880	[18]
46	$C_2H_2 + H + M \rightleftharpoons C_2H_3 + M$	11	1	1304	[18]
	Low pressure limit	40	-7	3312	
	Troe Parameters: a = 1, T*** = 1.00E-15,				
	T* = 675, T** = 1.00E+15				
47	$C_2H + H_2 \rightleftharpoons C_2H_2 + H$	6	2	435	[18]
48	$C_3H_6 \rightleftharpoons C_2H_2 + CH_4$	12	0	35249	[18]
49	$PC_3H_5 + H \rightleftharpoons C_3H_6$	14	0	0	[18]
50	$C_3H_6 + H \rightleftharpoons C_2H_4 + CH_3$	13	0	656	[18]
51	$C_3H_6 + H \rightleftharpoons AC_3H_5 + H_2$	5	3	1255	[18]
52	$C_3H_6 + H \rightleftharpoons PC_3H_5 + H_2$	6	3	6186	[18]
53	$C_3H_6 + CH_3 \rightleftharpoons AC_3H_5 + CH_4$	0	4	2858	[18]
54	$C_3H_6 + CH_3 \rightleftharpoons PC_3H_5 + CH_4$	0	4	6470	[18]
55	$AC_3H_5 + H \rightleftharpoons C_3H_6$	26	-4	2753	[18]
56	$PC_3H_5 + H \rightleftharpoons AC_3H_5 + H$	14	0	0	[18]
57	$H_2CCCH + H \rightleftharpoons C_3H_2 + H_2$	14	0	504	[24]
58	$H_2CCCH + CH_3 \rightleftharpoons C_3H_2 + CH_4$	13	0	0	[19]